
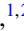



**Two-state model for critical points and the negative slope of the melting curve**Graeme J. Ackland <sup>1,\*</sup>, Hongxiang Zong <sup>1,2</sup>, Victor Naden Robinson <sup>1,3</sup>, Sandro Scandolo,<sup>3</sup> and Andreas Hermann<sup>1</sup><sup>1</sup>Centre for Science at Extreme Conditions and School of Physics and Astronomy,  
The University of Edinburgh, Edinburgh, EH9 3FD, United Kingdom<sup>2</sup>State Key Laboratory for Mechanical Behavior of Materials, Xi'an Jiaotong University, Xi'an, Shanxi 710049, China<sup>3</sup>The “Abdus Salam” International Centre for Theoretical Physics, I-34151 Trieste, Italy

(Received 15 March 2021; revised 12 July 2021; accepted 19 August 2021; published 30 August 2021)

We present a thermodynamic model which explains the presence of a negative slope in the melt curve, as observed in systems as diverse as the alkali metals and molecular hydrogen at high pressure. We assume that components of the system can be in one of two well defined states—one associated with low energy, the other with low volume. The model exhibits a number of measurable features which are also observed in these systems and are therefore expected to be associated with all negative Clapeyron-slope systems: first order phase transitions and thermodynamic anomalies along Widom lines. The melt curve maximum is a feature of the model, but appears well below the pressures where the change in state occurs in the solid: the solid-solid transition is related to the melt line minimum. An example of the model fitted to the electricle transition in potassium is discussed.

DOI: [10.1103/PhysRevB.104.054120](https://doi.org/10.1103/PhysRevB.104.054120)**I. INTRODUCTION**

Improvements in high-pressure and high-temperature experiments mean that the topic of liquid-liquid phase transitions has attracted significant attention recently. In particular, there are debates about whether a change in liquid structure can be regarded as a true phase transition, or a gradual crossover.

Determining this is challenging for either experiment or simulation. In a diamond anvil cell experiment it is near impossible to observe phase coexistence and be confident that the system has reached thermodynamic equilibrium. Indeed, many if not most high pressure experiments report phase coexistence across a range of pressures—something which is forbidden in equilibrium thermodynamics. The situation is no different in simulations—typical electronic structure calculations are done at a given pressure and temperature and “discontinuities” are inferred by extrapolation or, at best, hysteresis.

The melt curve for most materials has a positive slope on a  $PT$  phase diagram. This means that the liquid is less dense than the solid. There are exceptions, notably water is denser than ice, and other examples among elements include silicon, gallium, and carbon. These textbook exceptions at ambient pressure can generally be understood as due to the partial breakdown of a network of well defined covalent or hydrogen bonds causing the atoms or molecules in the liquid to have a higher coordination than the solid.

Another group of materials which have a negative Clapeyron slope at high pressure are the alkali metals [1–20]. Here the slope is typically positive at ambient pressure, reaching a maximum, then becoming negative in a pressure region where the solid phase is typically close packed. At still higher

pressures, there is a minimum in the melt curve before the slope becomes positive again. The solid phase in the region of negative slope is close packed, so the densification on melting cannot come from a collapsing open network. Curiously, hydrogen has a remarkably similar phase diagram to the alkalis which can be explained by competition between free rotors and quadrupole interactions [21–23].

Density functional theory can reproduce the negative slope [24–26]. It also shows some anomalous behavior in liquid heat capacity, compressibility, viscosity, and thermal expansion [27]. This implies that there is some significant change in the liquid binding, though whether it is a true transformation or a crossover remains unclear. As a consequence, there is renewed interest in analytic equations of state which can be fitted to data. For single phases, functional forms such as the Vinet equation of state work well, but many interesting phenomena occur where the equation of state is concave or discontinuous.

The thermodynamically stable state is the one with the lowest Gibbs free energy:

$$G(P, T) = U + PV - TS$$

taking  $P$  and  $T$  as the independent variables. Evidently  $G$  depends on three quantities, energy, density, and entropy. Any attempt to relate microscopic to macroscopic properties needs to consider all three, and how they vary between phases.

There are a wide range of approaches to describe complex high pressure structures. Those based on electronic-structure include electricle [5], two band [28,29], Fermi surface [30–32],  $s$ - $p$  [33] or  $s$ - $d$  [34] transfer, Mott transitions [35] or pairing [36], molecularization [37–39], high-low spin transition [40–42], polymerization [43], and “simple-complex” [44] transition types. Other approaches based on interatomic forces include soft-core [45,46] and associating particles [47,48].

Despite this huge variety of microscopic models, simple, analytic thermodynamic models for the melting point maxima [49–51] and liquid-liquid transformation are missing [52,53].

\*Corresponding author: [gjackland@ed.ac.uk](mailto:gjackland@ed.ac.uk)

Rapoport [54] implies that Klement built such a model, but it was never published—Rapoport’s own analysis of Klement’s model does not show a melting point maximum. A number of lattice-based approaches have been tried [55], but for obvious reasons their applicability to the fluid state is debatable. Makov has introduced a thermodynamic approach for continuous and discontinuous liquid transitions based on different heat capacities and compressibility, which also gives a negative melting line [56,57].

We note that most of the microscopic models are based on a trade-off between two types of interaction, one which has lower energy, the other lower volume. The purpose of this paper is to lay out the minimal requirements for an analytic model of a discontinuous liquid-liquid transformation and a melting point maximum based only on the idea that a material can adopt two different states.

The paper is structured as follows—we start by deriving thermodynamic results for heat capacity, expansivity, and compressibility in a convenient analytic form. We then present a mixing model between two thermodynamic states, demonstrating the Widom lines. A microscopic model inspired by the electricle transition [5–11,58–68], where the states differ only in volumes, is worked through in detail for both solid and liquid cases. It is shown that this model is sufficient to obtain the melt curve maximum, and can support a discontinuous phase transition in the liquid. A parametrization for potassium is presented.

## II. THERMODYNAMIC MODEL

The theory derived here is of very general applicability. However, we found it helpful to have a concrete microscopic model in mind as it is developed.

### A. Motivation from simple metals at pressure

We propose that the structure of the high-pressure alkali metals can be modeled as a mixture of two distinct electronic states: a low-pressure *s*-type free electron state, and a high-pressure “electricle” state, with electrons localized in interstitial pockets, referred to as pseudoanions. In the case of fcc, we can imagine that the octahedral site is the pseudoanion, so the electricle has a rocksalt structure. This should not be taken too literally because in reality, the electricle transition is accompanied by a crystal structural transformation. Similar evolution happens in a liquid, but here the transition is continuous because differently sized pseudoanion sites are available, and there is no symmetry. This microscopic picture can be related to a macroscopic one by considering the energy, volume, and entropy of the two states:

(1) The electricle has higher energy because the electron is confined away from the positively charged ion.

(2) The electricle has small volume, because it can occupy the interstitial site between ions, leading to more efficient packing.

(3) A mixture of the two states gives higher entropy.

In addition to the electricle transition, we may also compare solid and liquid phases for which the solid has lower energy and enthalpy, independent of the electricle fraction.

In the specific case of electricles, the entropy difference between the free-electron and electricle state is negligible [27]: in more general applications, one could consider different entropy in the two states, in addition to entropy of mixing and entropy of melting.

The need to describe  $U$ ,  $TS$ , and  $PV$  for each phase means that even the simplest model inevitably has several parameters.

### B. Thermodynamics

In a general two-state model, a Gibbs free energy is written as  $G(x, P, T)$  where  $x$  is the fraction of one of the two states. The equilibrium value for  $G(P, T)$  is obtained by minimizing  $G(x, P, T)$  with respect to  $x$ . So for all  $P, T$  we have

$$G(P, T) = \min_x G(x, P, T). \quad (1)$$

Thus  $x$  is a dependent variable whose value at equilibrium varies with the independent variables pressure and temperature. Values of  $x$  which do not minimize  $G(x, P, T)$  represent nonequilibrium states. A necessary, but not sufficient requirement for equilibrium is

$$\left(\frac{\partial G}{\partial x}\right)_{P,T} = \left(\frac{\partial H}{\partial x}\right)_{P,T} - T \left(\frac{\partial S}{\partial x}\right)_{P,T} = 0, \quad (2)$$

where  $H = U + PV$  is the enthalpy. Simply solving that equation will also generate unphysical free energy maxima and metastable states.

Thermodynamic properties are obtained as derivatives of the free energy. Although the calculus is routine, we present the results here because of the additional terms which arise due to the  $x$  factor, and the fact that some derivatives cannot be written analytically because of the requirement to minimize  $x$ .

#### 1. Heat capacity $C_p$

The standard thermodynamic definitions of the heat capacity are

$$C_p = \left(\frac{\partial H}{\partial T}\right)_P = T \left(\frac{\partial S}{\partial T}\right)_P = T \left(\frac{\partial^2}{\partial T^2} \min_x [G(x, P, T)]\right)_P. \quad (3)$$

Note that  $x$  is not an independent variable, and changes in  $x$  contribute to the heat capacity

$$C_p = \left(\frac{\partial H}{\partial T}\right)_{P,x} + \left(\frac{\partial H}{\partial x}\right)_P \left(\frac{\partial x}{\partial T}\right)_P. \quad (4)$$

The quantity  $\frac{\partial T}{\partial x}$  can be awkward to evaluate, so to eliminate it, we consider

$$\left(\frac{\partial}{\partial T}\right) \left(\frac{\partial G}{\partial x}\right) = -\left(\frac{\partial S}{\partial x}\right) + \left(\frac{\partial x}{\partial T}\right) \left[\left(\frac{\partial^2 G}{\partial x^2}\right)\right], \quad (5)$$

dropping the subscripts for clarity. Using the equilibrium condition [Eq. (2)], this gives

$$\left(\frac{\partial T}{\partial x}\right)_P = T \left(\frac{\partial^2 G}{\partial x^2}\right)_P / \left(\frac{\partial H}{\partial x}\right)_P. \quad (6)$$

From which the expression for the heat capacity becomes

$$C_P = \left( \frac{\partial H}{\partial T} \right)_P = \left( \frac{\partial H}{\partial T} \right)_{P,x} + \frac{1}{T} \left( \frac{\partial H}{\partial x} \right)_P \bigg/ \left( \frac{\partial^2 G}{\partial x^2} \right)_P. \quad (7)$$

## 2. Isothermal compressibility

The standard thermodynamic definitions of compressibility are

$$\kappa_T = -\frac{1}{V} \left( \frac{\partial V}{\partial P} \right)_T = -\frac{1}{V} \left( \frac{\partial^2 G}{\partial P^2} \right)_T, \quad (8)$$

including the internal variable  $x$ ,

$$\left( \frac{\partial^2 G}{\partial P^2} \right)_T = \left( \frac{\partial^2 G}{\partial P^2} \right)_{T,x} + 2 \left( \frac{\partial^2 G}{\partial P \partial x} \right)_T \left( \frac{\partial x}{\partial P} \right)_T. \quad (9)$$

The equilibrium condition ensures that the  $\left( \frac{\partial G}{\partial x} \right)_T \left( \frac{\partial^2 x}{\partial P^2} \right)_T$  term is zero.

Again, there is no convenient relationship between  $P$  and  $x$ , but following a similar argument to Eq. (6) we find

$$\left( \frac{\partial x}{\partial P} \right)_T = - \left( \frac{\partial^2 G}{\partial P \partial x} \right)_T \bigg/ \left( \frac{\partial^2 G}{\partial x^2} \right)_T \quad (10)$$

and

$$\begin{aligned} \left( \frac{\partial^2 x}{\partial P^2} \right)_T &= \left( \frac{\partial^3 G}{\partial P^2 \partial x} \right)_T \bigg/ \left( \frac{\partial^2 G}{\partial x^2} \right)_T \\ &\quad - \left( \frac{\partial^3 G}{\partial P \partial x^2} \right)_T \bigg/ \left( \frac{\partial^2 G}{\partial x^2} \right)_T. \end{aligned} \quad (11)$$

## 3. Thermal expansion

The standard thermodynamic definitions of thermal expansion are

$$\alpha = \frac{1}{V} \left( \frac{\partial V}{\partial T} \right)_T = \frac{1}{V} \left( \frac{\partial^2 G}{\partial T \partial P} \right), \quad (12)$$

$$\begin{aligned} \frac{\partial^2 G}{\partial T \partial P} &= \left( \frac{\partial^2 G}{\partial T \partial P} \right)_x + \left( \frac{\partial^2 G}{\partial P \partial x} \right)_T \left( \frac{\partial x}{\partial T} \right)_P \\ &\quad + \left( \frac{\partial^2 G}{\partial T \partial x} \right)_P \left( \frac{\partial x}{\partial P} \right)_T. \end{aligned} \quad (13)$$

Again, using the equilibrium condition  $\left( \frac{\partial G}{\partial x} \right)_T = 0$ .

### C. Linear combination model with ideal solution

In a slightly more specific model, a system is described by particles in two possible thermodynamic states  $A$  ( $x = 1$ ) and  $B$  ( $x = 0$ ). When mixed in an ideal solution, the Gibbs free energy is given by

$$\begin{aligned} G(P, T) &= xG(1, P, T) + (1-x)G(0, P, T) \\ &\quad + RT[x \ln x + (1-x) \ln(1-x)], \end{aligned} \quad (14)$$

where  $x$  is the fraction of particles in state  $A$ ,  $G_A = G(1, P, T)$  and  $G_B = G(0, P, T)$  are the Gibbs free energies of pure  $A$  and  $B$  states. The equilibrium value for  $x$  is found by minimizing  $G(P, T)$ :

$$x(P, T) = \frac{e^{-G_A/RT}}{e^{-G_A/RT} + e^{-G_B/RT}} = \frac{1}{1 + e^{-\Delta G/RT}}, \quad (15)$$

with  $\Delta G = G_B - G_A$ .

We can find the volume

$$V(P, T) = \left( \frac{\partial G}{\partial P} \right)_T = xV_A(P, T) + (1-x)V_B(P, T) \quad (16)$$

and entropy

$$\begin{aligned} S(P, T) &= - \left( \frac{\partial G}{\partial T} \right)_P = xS_A(P, T) + (1-x)S_B(P, T) \\ &\quad + R[x \ln x + (1-x) \ln(1-x)] \end{aligned} \quad (17)$$

always remembering that  $x = x(P, T)$ . We further derive analytic expressions for compressibility

$$\kappa_T = -\frac{1}{V} \left( \frac{\partial V}{\partial P} \right)_T = x\kappa_{T,A} + (1-x)\kappa_{T,B} + \frac{\Delta V}{V} \left( \frac{\partial x}{\partial P} \right)_T, \quad (18)$$

with  $\Delta V = V_B - V_A$  and thermal expansion

$$\alpha = \frac{1}{V} \left( \frac{\partial V}{\partial T} \right)_P = x\alpha_{T,A} + (1-x)\alpha_{T,B} + \frac{\Delta V}{V} \left( \frac{\partial x}{\partial T} \right)_P. \quad (19)$$

Both of which have an anomalous component arising from the conversion of material between the two states, in addition to the weighted average. For the heat capacity there is an additional anomalous term from the mixing entropy

$$\begin{aligned} C_P &= T \left( \frac{\partial S}{\partial T} \right)_P \\ &= xC_{P,A} + (1-x)C_{P,B} + \left( \Delta S + R \ln \frac{x}{1-x} \right) \left( \frac{\partial x}{\partial T} \right)_P, \end{aligned} \quad (20)$$

with  $\Delta S = S_B - S_A$ .

From Eq. (15) we immediately see that there is no discontinuity in  $x$ , from which it follows that this model cannot describe a phase transition, only a crossover. We also observe that the ideal solution entropy ensures that mathematically, as well as intuitively,  $0 < x < 1$ .

## D. Nonideal solution solid model

A small rephrasing of the Bragg-Williams (BW) [69] model can be used to extend the model from Sec. II C to describe a discontinuous transition within a single solid phase. BW is a mean field approximation to the Ising model, where for high-pressure applications the spins are mapped to “electride” and “free electron” states, and the “field” is mapped to the enthalpy difference between the two states. Although the model has wider applicability, e.g., the high-spin/low-spin transition in ferrous minerals, we will use the electride terminology here.

The enthalpy difference with respect to the  $x = 0$  free electron state is

$$H = x(\Delta U_e + P\Delta V_e) + Jx(1-x), \quad (21)$$

where  $x$  is the electride fraction,  $\Delta U_e$  and  $\Delta V_e$  are the change in energy and volume with respect to the free electron values

when an electron moves to an electrone pseudoanion site, both assumed positive, and  $J$  is a local coupling between electrone and free electron. A high pressure phase transition at  $T = 0$  occurs when the field/enthalpy difference changes sign ( $P_T = \Delta U/\Delta V$ ).

Including entropy, the Gibbs free energy relative to the free electron state is

$$G_{\text{BW}} = x(\Delta U_e - P\Delta V_e - T\Delta S_e) + Jx(1-x) + RT[x\ln x + (1-x)\ln(1-x)]. \quad (22)$$

We find that the  $x$ -dependent contributions to relative volume, internal energy, and entropy are

$$V = -x\Delta V_e, \quad (23)$$

$$U = x\Delta U_e + Jx(1-x), \quad (24)$$

$$S = R[x\ln x + (1-x)\ln(1-x)] + \Delta S_e. \quad (25)$$

We obtain these results by differentiating  $G$ . This is not completely trivial, as they rely on the stationary property of  $G(x)$  at equilibrium [Eq. (2)].

We now find

$$\frac{\partial H}{\partial x} = (\Delta U_e - P\Delta V_e) + J(1-2x), \quad (26)$$

$$\frac{\partial G}{\partial x} = (\Delta U_e - P\Delta V_e - T\Delta S_e) + RT\ln[x/(1-x)] + J(1-2x), \quad (27)$$

$$\frac{\partial^2 G}{\partial x^2} = \frac{RT}{x(1-x)} - 2J, \quad (28)$$

$$C_P(x) = \frac{1}{T} \frac{[\Delta U_e - P\Delta V_e + J(1-2x)]^2}{\frac{RT}{x(1-x)} - 2J}. \quad (29)$$

We can see immediately that the heat capacity has a discontinuity if  $RT/2J = x(1-x)$ , and since  $x(1-x)$  must lie between 0 and 1/4, a discontinuous phase transition occurs for any  $T < J/2R$  at  $P = \Delta U_e/\Delta V_e$ . Interestingly, along a line above the critical point, the contribution to  $C_P$  goes to zero.

If it seems odd that  $V$  and  $U$  go to zero, at high and low pressures, remember that the full free energy of the system will include terms independent of  $x$ , representing the equation of state of a reference ( $x = 0$ ) material. To compare with a real system, one needs to add an  $x$ -independent free energy  $G_{\text{ref}}(P, T)$  to Eq. (22) which adds a smoothly varying additional term to all quantities.

Bragg and Williams considered an atomic level system [69], and so assumed that the two sites have equal entropy; in applications such as polymerization or atomic-molecular transitions where the number of independent objects changes a further term  $T\Delta S_e$  could be added to relax this assumption. This introduces a slope to the phase boundary and additional tilt to the Widom line, but does not change the general picture.

Bragg-Williams' solid-solid model is conceived for alloy order-disorder rather than pressure. However, a similar con-

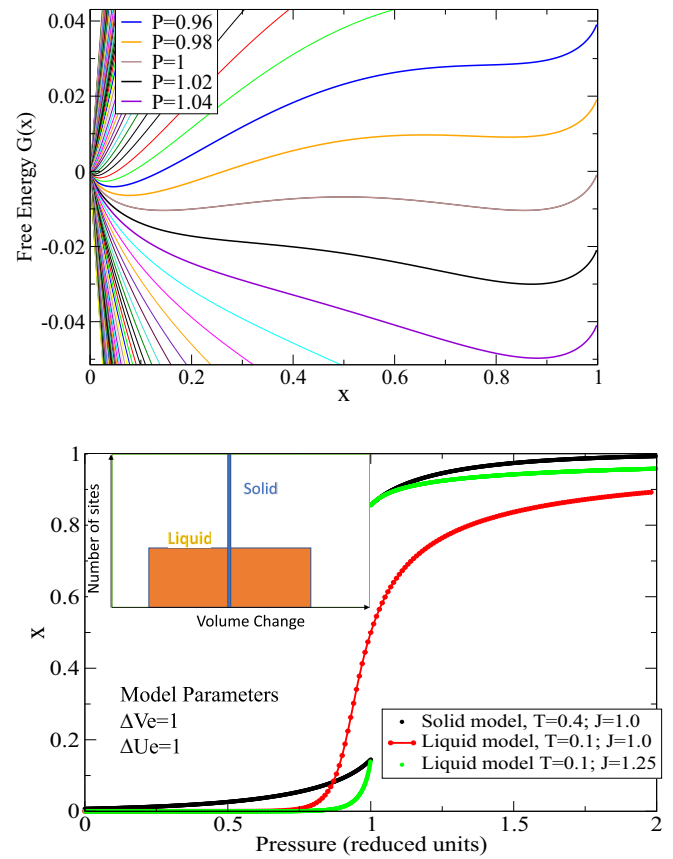


FIG. 1. (Top) Variation of free energy with  $x$  for the liquid model with  $\Delta V_e = 1$ ,  $\Delta U_e = 1$ ,  $J = 1.25$  at  $T = 0.1$ . Lines correspond to different pressures with selected values around the transition at  $P = 1$  highlighted. The equilibrium value of  $x$  corresponds to the free energy minimum. These conditions permit a first order transformation, and a metastable state can be seen for  $P = 0.98$ . (Bottom) Variation of fraction of two states ( $x$ ) for solid and liquid models, with identical energy and volume differences. At reduced  $T = 0.4$  the solid already exhibits a discontinuous phase transition, while the liquid does not ( $T = 0.1$  shown). If  $J$  is increased from 1.0 to 1.25, the liquid model also exhibits a phase transition. The chosen values of  $\Delta U_e = 1$ ;  $\Delta V_e = 1$  mean that the transition pressure is at  $P = 1$  in either model. Inset: Schematic showing the different volume changes available in liquid (orange) compared with unique value in solid (blue, delta function).

cept can be applied to the high-spin low-spin crossover in iron oxides [40,70]. The present model allows for an isostructural phase transition at low temperature, as well as a crossover: such a true phase transition, an associated critical point, would require a coupling  $J$  between sites which disfavored mixing. This coupling may come from short ranged strain [41,42], magnetic spin coupling or from phonons [71], or be calculated directly from first principles [70], and may vary with pressure [72]. Magnetowüstite (Mg,Fe)O and perovskite (Mg,Fe)SiO<sub>3</sub> in the iron rich regime are prime candidates. They are known to pronounced anomalies in heat capacity, and compressibility, but from experiment and DFT calculations these system appear to exhibit a crossover [73–76], suggesting the spin coupling either favors mixing or is so weak that the transition is below the studied temperatures.

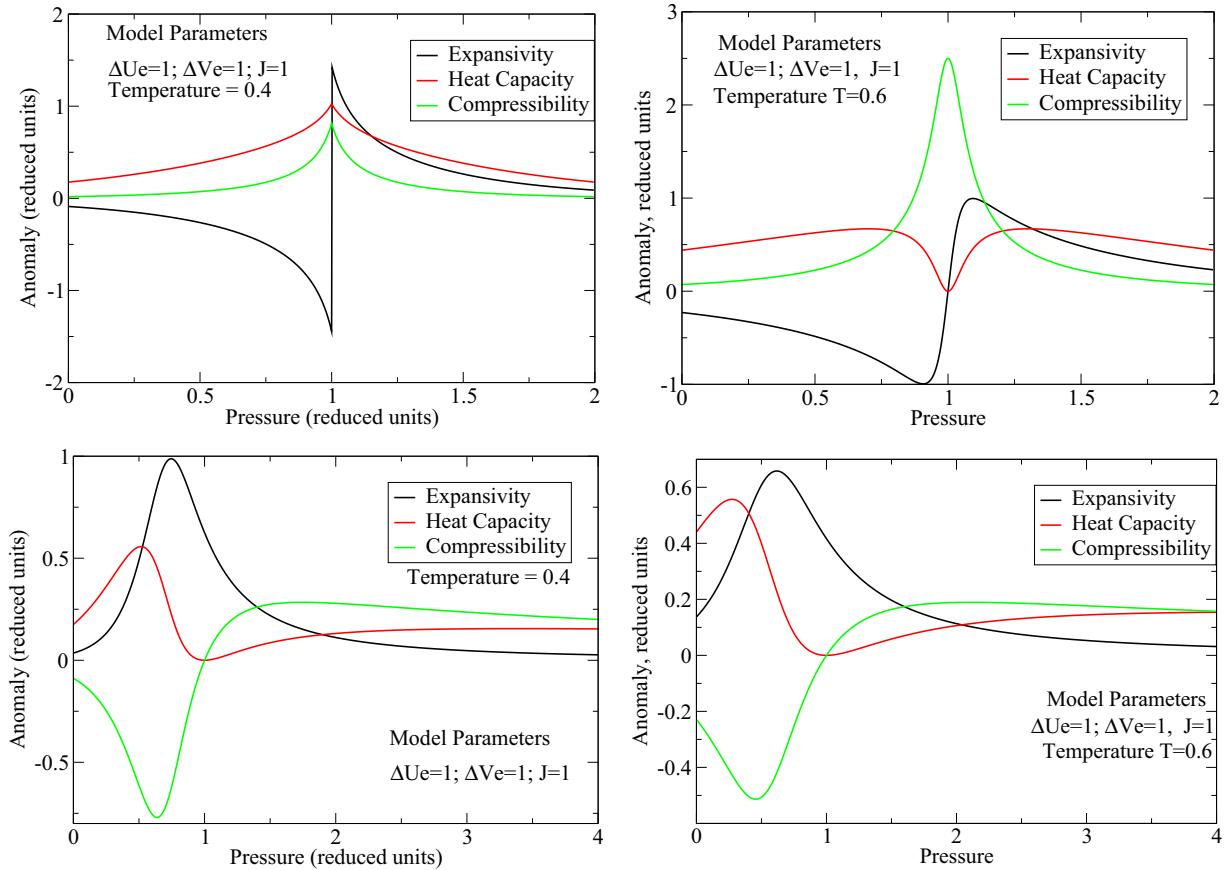


FIG. 2. Thermodynamic anomalies due to Bragg-Williams-type solid model (top) and liquid model (bottom) for  $T = 0.4$  and  $T = 0.6$ . With parameters set to unity, so that the solid critical temperature is 0.5 and the phase line is vertical at  $P = 1$ .

### E. Two-site electricle liquid model

Our liquid model differs from the solid in just one detail: we assume there are a range of different possible electricle sites, each entailing different volume changes  $\Delta V$  (see Fig. 1, inset). This contrasts with the crystal model, in which the available electricle sites are equivalent by symmetry.

For simplicity we assume that the electricle sites are such that the change in volume entailed in occupying them is linearly distributed and range from  $-2\Delta V_e$  to  $+2\Delta V_e$ . Note that a positive  $\Delta V$  implies that the electricle would increase the volume, so such sites will never be occupied.

With finite electricle fraction  $x$ , those sites offering the largest volume reduction will be occupied. The total volume change is calculated by integrating over the volumes changes of the individual occupied sites:

$$\Delta V = \int_0^x 2\Delta V_e(x' - 1)dx' = \Delta V_e(x^2 - 2x), \quad (30)$$

where the upper bound on the integral indicates that sites which would increase the overall volume are not occupied.

The excess Gibbs free energy, relative to the free electron liquid, is thus

$$G_{EL}(x) = x\Delta U_e - x(2-x)P\Delta V_e + Jx(1-x) + k_B T [x \ln x + (1-x) \ln(1-x)]. \quad (31)$$

There are now nonlinearities in relative energy, entropy, and density:

$$\begin{aligned} V &= -x(2-x)\Delta V_e, \\ U &= x\Delta U + Jx(1-x), \\ S &= R[x \ln x + (1-x) \ln(1-x)]. \end{aligned} \quad (32)$$

We now find

$$\frac{\partial H}{\partial x} = [\Delta U_e - (2-2x)P\Delta V_e] + J(1-2x), \quad (33)$$

$$\begin{aligned} \frac{\partial G}{\partial x} &= [\Delta U_e - (2-2x)P\Delta V_e] \\ &+ RT \ln[x/(1-x)] + J(1-2x), \end{aligned} \quad (34)$$

$$\frac{\partial^2 G}{\partial x^2} = 2P\Delta V_e + \frac{RT}{x(1-x)} - 2J, \quad (35)$$

$$C_P = \frac{1}{T} \frac{[\Delta U_e - (2-2x)P\Delta V_e + J(1-2x)]^2}{\frac{RT}{x(1-x)} - 2J + 2P\Delta V_e}. \quad (36)$$

This model does not necessarily have a critical point: the entropic and volume terms are always convex, so only the demixing  $J$  term can drive phase separation. Whether this happens depends on the value of  $P$  at the putative phase boundary  $x = \frac{1}{2}$ , giving  $P = \Delta U_e/\Delta V_e$ .

These quantities are plotted in Fig. 2, where it is again clear that the model predicts a peak in specific heat and

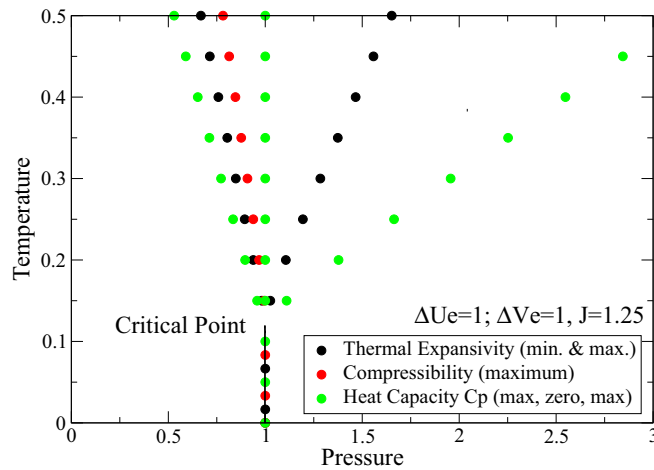


FIG. 3. Phase diagram for the liquid model with parameters as shown ( $\Delta S = 0$  if nonzero then the phase transition line has a slope). Points are the calculated maxima and minimum of the thermodynamic anomalies in compressibility, expansivity, and heat capacity. The first order transition between low- and high- $x$  liquids ends in a critical point: in application of the model to real materials, this critical point may lie below the melt line. Above the critical temperature, the extrema of the thermodynamic properties trace out the Widom lines which converge and end at the critical point.

compressibility, along with a dip in the thermal expansivity. These extrema trace out the Widom lines of the phase diagram (Fig. 3). It is important to note that this phase diagram includes only the two-site Hamiltonian: the underlying free energy of the  $x = 1$  and  $x = 0$  states is ignored.

Free energy variation with  $x$  is shown in Fig. 1, for a range of pressures around the phase transition. Below  $T_c$  there are two minima, degenerate at  $P = \Delta U_e / \Delta V_e$ , indicating a first order phase transition. An analytic estimate of  $T_c$  can be obtained from  $\frac{\partial^2 G}{\partial x^2} = 0$  or from setting  $x = 1/2$ . Note that the existence of the critical point requires two nonlinear terms in  $G$ , coming here from the entropy and the interaction energy. Figure 1 (lower) shows that  $x$  changes discontinuously along an isotherm at the transformation, in either the solid or liquid model. Notice that, for equivalent parameters, the critical point in the liquid falls at a lower  $T_c$  than for the solid.

If the liquid structure cannot accommodate enough potential electrone sites, the model can be extended to a maximum electrone fraction  $f$ . This would result in a change of the  $P\Delta V_e$  prefactor from  $x(2-x)$  to  $x(2-x/f)$ , but this additional complication makes no difference to the general argument, so hereinafter we take  $f = 1$ .

Positive  $J$  generates a first order transition with a critical point. The phase line is vertical (at  $P = \Delta U_e / \Delta V_e$ ) and ends at the critical temperature  $T_c$ . Note that the high pressure phase transition we are describing corresponds to the Ising spin-up  $\rightarrow$  spin-down transition, not the usual BW paramagnetic one.

Above the critical temperature there are anomalies in several observables, as shown in Fig. 2. The extreme values (Widom lines) for various properties do not fall in the same place: any definition of the supercritical transition pressure depends on which property is considered.

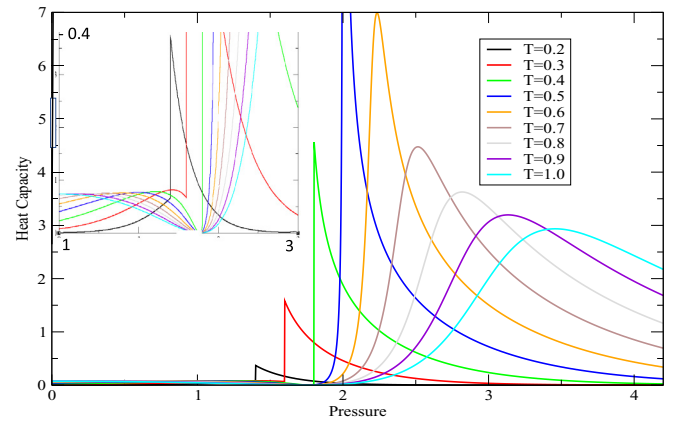


FIG. 4. Thermodynamic anomalies in the heat capacity for solid model with  $\Delta V_e = 1$ ,  $\Delta U_e = 1$ ,  $J = 1$ ,  $\Delta S = 2$ . Inset shows expanded view of low pressure region, with the same colors and heat capacity extending to 0.4 as shown.

## F. Entropy-driven transformation

So far we have considered models where the difference between the two phases is in the enthalpy. In other cases, such as the molecular-atomic transition in hydrogen, there is a significant change in entropy between the two states—in the hydrogen case because the number of particles doubles.

The addition of an  $x$ -dependent entropy term gives a slope to the phase boundary, and a similar change of slope to the Widom lines: some of which can even have the opposite slope to the phase boundary. From the Clausius-Clapeyron equation, the slope of the phase boundary is  $\frac{dP}{dT} = \Delta S / \Delta V$ . Exactly similar to the volume change, a linear dependence of entropy with  $x$  does not create a first order transition, the lowest order term which can do so is  $x(1-x)\Delta S$ . Such entropic demixing occurs in models with hard-core cubes and spheres [55,77,78],

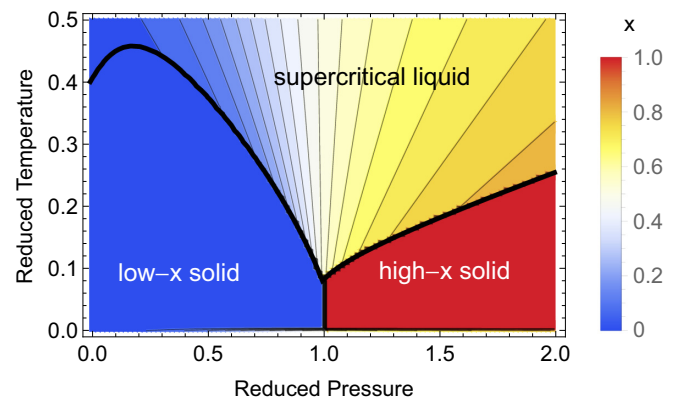


FIG. 5. Phase diagram for the combined solid-liquid two-site model with  $\Delta V_e = 1$ ,  $\Delta U_e = 1$ ,  $\Delta S = 0$ ,  $J = 1$  in both phases, and a linear free energy difference  $\Delta G_{sl} = 0.02 + 0.04P - 0.05T$  for the nonanomalous contributions. Data were collected by scanning a dense grid in  $P$ - $T$  space and plotting points where the free energy difference was less than 0.0005, in reduced units. Variation of  $x$  across the phase diagram is shown as a color map, from blue ( $x = 0$ ) to red ( $x = 1$ ).

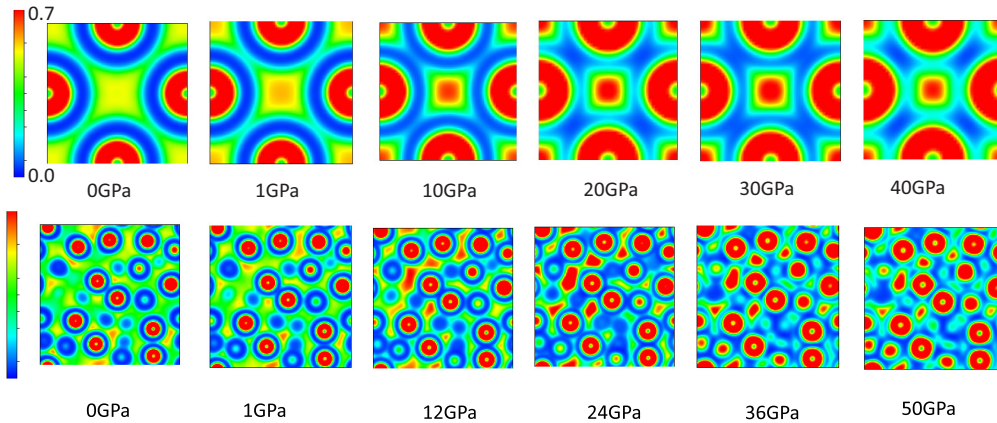
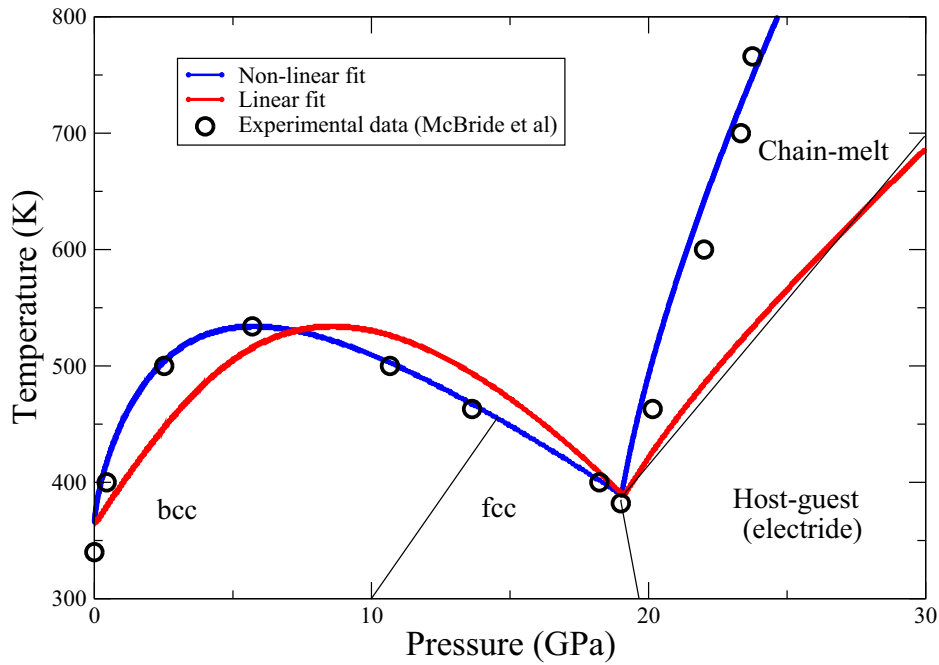


FIG. 6. Model fitted to potassium. (Upper) The phase diagram based on the two-state model used parameters  $\Delta U_e = 1.15$ ,  $\Delta V_e = 1$ ,  $J = 1$ ,  $\Delta S = -0.5$ , the same in both solid and liquid phases. The  $x$ -independent free energy difference between solid and liquid phases is  $\Delta G_{sl} = 0.12 + 0.24P - 0.33T$ . (Lower) Sequence of images showing the transition to electride state in fcc and liquid potassium. The figure shows an electron localization function (ELF) [89] calculated using CASTEP density functional code [90]. Red shows a region of high ELF and localized charge (see scale bar for values). The solid electride site is located at the  $(\frac{1}{2}, \frac{1}{2}, \frac{1}{2})$  position—center of the figure. The “liquid” image is a slice from a molecular dynamics snapshot [27] cutting through several atomic sites (red circles at 0 GPa—not all lie in the plane), and then rerun at several densities using the same fractional atomic positions. The interstitial regions, initially green (free electronlike) become increasingly red and blue as the electrons localize.

and has been claimed experimentally in supercooled water [79].

The heat capacity model with  $\Delta S = 2$  is illustrated in Fig. 4, showing the lambda profile of the discontinuous transition changing to the broad peak above the critical point. The gradient of the Clapeyron slope is evident from the shift of the lambda peak to higher pressure. The inset shows the peak in heat capacity in the low- $x$  phase.

### G. Two-site model for liquid-solid transformation

We can extend the two-site model to compare liquid and solid phases and calculate a melt line. This requires us to

consider the  $x$ -independent contributions to the free energy. A full equation of state is required for the nonanomalous contributions to  $C_p$ ,  $\alpha$ , and  $\kappa_T$ , however, to calculate the phase boundary, we need only know the free energy *difference* of  $x$ -independent contributions to the solid-liquid free energy  $\Delta G_{sl}$ .

Thus we have an equation for the phase boundary

$$\Delta G_{sl}(P, T) = G^l(x_l, P, T) - G^s(x_s, P, T), \quad (37)$$

where  $x_l(P, T)$  and  $x_s(P, T)$  are the equilibrium values of  $x$  in liquid and solid, respectively, calculated by minimizing the free energy  $G(P, T)$  at each  $P, T$  point.

In Fig. 5 we show an illustrative example with a zero pressure melting point at  $T = 0.4$  and a positive Clapeyron slope of 0.8, in reduced units.

To illustrate the model, we use the same  $x$ -dependent parameters  $\Delta V = 1$ ,  $\Delta U = 1$ ,  $\Delta S = 0$ ,  $J = 1$  in both liquid and solid. This means that  $x$ -dependent terms in free energy for solid and liquid models are equal in the  $x \rightarrow 0$  and  $x \rightarrow 1$  limits. For the  $x$ -independent terms, we assume that energy, entropy, and density differences between solid and liquid are constant.

This choice of parameters means that the solid-solid phase line is vertical ( $\Delta S = 0$ ) and there is no discontinuous liquid-liquid transition. This is similar to the case of the simple metals. A significantly larger value of  $J$  would be needed to extend the phase boundary into the liquid region, as shown in Fig. 3. A nonzero  $\Delta S$  leads to a slope in the phase boundary, but does not change the general picture.

The figure also shows how  $x$  varies across the phase diagram—gradually in the liquid, but discontinuously in the solid.

#### H. Example: Application to potassium

The high pressure crystallography and reentrant melt curve of potassium have been determined experimentally [4,80,81]. DFT calculations show an electrone transition in potassium as in other simple metals [5–10,82]. Liquid potassium calculations suggest a number of irregularities [27] in the thermodynamic properties which cannot be fitted by smoothly varying models [83].

Figure 6 shows an *ab oculo* parametrization of the liquid-solid transformation model to this data, with a simple linear model for  $x$ -independent terms. The reduced units of the model correspond to 20 GPa and 1000 K for potassium. While the overall shape is reproduced with a linear fit, the low pressure melt curve appears parabolic and the high pressure line is not sufficiently steep. The fit can be significantly improved by introducing a nonlinear equation of state, such that  $P^* \rightarrow P^{3/2}$ , and is reduced by a factor of 5 above the transition.

Curiously, the unadjusted high-pressure melt line of the linear model follows the chain-melting line, in which the guest atoms in the solid phase III melt [4,26].

It is notable that the melting line minimum is coincident with the triple point of the solid-solid transformation from fcc to host-guest structure, which has been associated with the electrone transition [5,7,26]. The melting point maximum has no such association, which casts doubt on the extrapolation of the fcc-bcc line to the melt curve maximum, which has been drawn and copied without evidence in, e.g., lithium [13,14,84–86]. In fact, the 180° rule means that it is thermodynamically impossible for a solid-solid phase line to intercept

the melt curve at a point of negative curvature such as a maximum.

### III. DISCUSSION

We have presented a simple analytic model which explains the anomalous shape of the melt line observed in many high pressure systems. The key features required are

- (1) A microscopic mechanism by which the atoms can reduce their volume, at the expense of increasing their energy.
- (2) Disorder in the liquid leading to wider range of possible atomic environments compared to the solid.

We have shown that a discontinuous phase transformation can be driven by a repulsion between the two states, analogous to the  $Jx(1-x)$  term in the Bragg-Williams model. This repulsion may be either enthalpic or entropic, but must introduce negative curvature to  $G(x)$ : terms linear in  $x$  cannot result in a discontinuous transition.

The discontinuous transitions in the model do not depend on changes in crystal symmetry. In reality, it is likely that a discontinuous change in the type of electronic binding of a solid will also be accompanied by a symmetry change. Thus even in principle the solid-solid critical point can occur only for isostructural transitions such as hydrogen and cerium [35,87,88].

Above the critical point, the model predicts a series of experimentally measurable “Widom lines” associated with anomalies of thermodynamic properties. These occur for all parametrizations, even where there is no critical point, or there is a liquid-liquid critical point which lies below the melt line.

By comparing free energy models for crystal and liquid phases, we constructed a melt line from this model. This has a characteristic minimum at the point where the two-state mixing entropy is maximized ( $x = \frac{1}{2}$ ), coincident with the solid-solid phase transformation. Combined with a positive slope at low pressures, this means that there must also be a melting temperature maximum which, curiously, does not appear to be coincident with other features in the phase diagram.

The model has been applied to the melt curve of potassium, using a very simple linear fitting scheme. More accurate fitting to other materials would be straightforward, and the model framework has broad application for producing equations of state for any material with a complex liquid-liquid transformation.

#### ACKNOWLEDGMENTS

H.Z. and G.J.A. acknowledge the ERC project HECATE for funding. H.Z. thanks the National Natural Science Foundation of China (51931004 and 51871177). Computing resources were obtained via the UKCP EPSRC Grant No. EP/P022561/1. We thank X. Ding and H Ehteshami for useful discussions.

[1] K. Tsuji, K. Yaoita, M. Imai, T. Mitamura, T. Kikegawa, O. Shimomura, and H. Endo, Pressure-induced structural change of liquid cesium, *J. Non. Cryst. Solids* **117-118**, 72 (1990).

[2] K. Tsuji, Y. Katayama, Y. Morimoto, and O. Shimomura, Structure of liquid rubidium under high pressure, *J. Non. Cryst. Solids* **205-207**, 295 (1996).



- [3] S. Falconi, M. I. McMahon, L. F. Lundegaard, C. Hejny, R. J. Nelmes, and M. Hanfland, X-ray diffraction study of diffuse scattering in incommensurate rubidium-IV, *Phys. Rev. B* **73**, 214102 (2006).
- [4] E. E. McBride, K. A. Munro, G. W. Stinton, R. J. Husband, R. Briggs, H.-P. Liermann, and M. I. McMahon, One-dimensional chain melting in incommensurate potassium, *Phys. Rev. B* **91**, 144111 (2015).
- [5] M. Marqués, G. J. Ackland, L. F. Lundegaard, G. Stinton, R. J. Nelmes, M. I. McMahon, and J. Contreras-García, Potassium under Pressure: A Pseudobinary Ionic Compound, *Phys. Rev. Lett.* **103**, 115501 (2009).
- [6] M. Gatti, I. V. Tokatly, and A. Rubio, Sodium: A Charge-Transfer Insulator at High Pressures, *Phys. Rev. Lett.* **104**, 216404 (2010).
- [7] G. Woolman, V. Naden-Robinson, M. Marqués, I. Loa, G. J. Ackland, and A. Hermann, Structural and electronic properties of the alkali metal incommensurate phases, *Phys. Rev. Mater.* **2**, 053604 (2018).
- [8] M. Marqués, M. Santoro, C. L. Guillaume, F. A. Gorelli, J. Contreras-García, R. T. Howie, A. F. Goncharov, and E. Gregoryanz, Optical and electronic properties of dense sodium, *Phys. Rev. B* **83**, 184106 (2011).
- [9] L. Zhao, H. Zong, X. Ding, J. Sun, and G. J. Ackland, Commensurate-incommensurate phase transition of dense potassium simulated by machine-learned interatomic potential, *Phys. Rev. B* **100**, 220101(R) (2019).
- [10] M.-S. Miao and R. Hoffmann, High pressure electrides: A predictive chemical and physical theory, *Acc. Chem. Res.* **47**, 1311 (2014).
- [11] M. Frost, A. L. Levitan, P. Sun, and S. Glenzer, Equation of state and electron localisation in fcc lithium, *J. Appl. Phys.* **123**, 065901 (2018).
- [12] M. Frost, J. B. Kim, E. E. McBride, J. R. Peterson, J. S. Smith, P. Sun, and S. H. Glenzer, High-Pressure Melt Curve and Phase Diagram of Lithium, *Phys. Rev. Lett.* **123**, 065701 (2019).
- [13] A. M. J. Schaeffer, W. B. Talmadge, S. R. Temple, and S. Deemyad, High Pressure Melting of Lithium, *Phys. Rev. Lett.* **109**, 185702 (2012).
- [14] C. L. Guillaume, E. Gregoryanz, O. Degtyareva, M. I. McMahon, M. Hanfland, S. Evans, M. Guthrie, S. V. Sinogeikin, and H.-K. Mao, Cold melting and solid structures of dense lithium, *Nat. Phys.* **7**, 211 (2011).
- [15] E. Gregoryanz, L. F. Lundegaard, M. I. McMahon, C. Guillaume, R. J. Nelmes, and M. Mezouar, Structural diversity of sodium, *Science* **320**, 1054 (2008).
- [16] H. Eshet, R. Z. Khaliullin, T. D. Kühne, J. Behler, and M. Parrinello, Microscopic Origins of the Anomalous Melting Behavior of Sodium Under High Pressure, *Phys. Rev. Lett.* **108**, 115701 (2012).
- [17] Q.-J. Hong and A. van de Walle, Reentrant melting of sodium, magnesium, and aluminum: General trend, *Phys. Rev. B* **100**, 140102(R) (2019).
- [18] C.-S. Zha and R. Boehler, Melting of sodium and potassium in a diamond anvil cell, *Phys. Rev. B* **31**, 3199 (1985).
- [19] O. Narygina, E. E. McBride, G. W. Stinton, and M. I. McMahon, Melting curve of potassium to 22 GPa, *Phys. Rev. B* **84**, 054111 (2011).
- [20] D. Karton and G. Makov, Structural and electronic transition in liquid rubidium, *Phys. Rev. B* **103**, 024103 (2021).
- [21] I. B. Magdău, M. Marqués, B. Borgulya, and G. J. Ackland, Simple thermodynamic model for the hydrogen phase diagram, *Phys. Rev. B* **95**, 094107 (2017).
- [22] H. Zong, H. Wiebe, and G. J. Ackland, Understanding high pressure molecular hydrogen with a hierarchical machine-learned potential, *Nat. Commun.* **11**, 5014 (2020).
- [23] S. van de Bund and G. J. Ackland, Quadrupole arrangements and the ground state of solid hydrogen, *Phys. Rev. B* **101**, 014103 (2020).
- [24] E. R. Hernández, A. Rodríguez-Prieto, A. Bergara, and D. Alfe, First-Principles Simulations of Lithium Melting: Stability of the Bcc Phase Close to Melting, *Phys. Rev. Lett.* **104**, 185701 (2010).
- [25] Y. Feng, J. Chen, D. Alfè, X.-Z. Li, and E. Wang, Nuclear quantum effects on the high pressure melting of dense lithium, *J. Chem. Phys.* **142**, 064506 (2015).
- [26] V. N. Robinson, H. Zong, G. J. Ackland, G. Woolman, and A. Hermann, On the chain-melted phase of matter, *Proc. Natl. Acad. Sci. USA* **116**, 10297 (2019).
- [27] H. Zong, V. N. Robinson, A. Hermann, L. Zhao, S. Scandolo, X. Ding, and G. J. Ackland, Free electron to electride transition in dense liquid potassium, *Nat. Phys.* **17**, 955 (2021).
- [28] G. J. Ackland and S. K. Reed, Two-band second moment model and an interatomic potential for caesium, *Phys. Rev. B* **67**, 174108 (2003).
- [29] G. J. Ackland, Two-band second moment model for transition metals and alloys, *J. Nucl. Mater.* **351**, 20 (2006).
- [30] V. F. Degtyareva, Brillouin zone concept and crystal structures of *sp* metals under high pressure, *High Press. Res.* **23**, 253 (2003).
- [31] G. J. Ackland and I. R. Macleod, Origin of the complex crystal structures of elements at intermediate pressure, *New J. Phys.* **6**, 138 (2004).
- [32] V. F. Degtyareva, Simple metals at high pressures: The Fermi sphere–Brillouin zone interaction model, *Phys. Usp.* **49**, 369 (2006).
- [33] Y. Ma, M. Eremets, A. R. Oganov, Y. Xie, I. Trojan, S. Medvedev, A. O. Lyakhov, M. Valle, and V. Prakapenka, Transparent dense sodium, *Nature (London)* **458**, 182 (2009).
- [34] S. K. Reed and G. J. Ackland, Theoretical and Computational Study of High-Pressure Structures in Barium, *Phys. Rev. Lett.* **84**, 5580 (2000).
- [35] B. Johansson, The  $\alpha$ - $\gamma$  transition in cerium is a Mott transition, *Philos. Mag.* **30**, 469 (1974).
- [36] J. B. Neaton and N. W. Ashcroft, Pairing in dense lithium, *Nature (London)* **400**, 141 (1999).
- [37] N. Ashcroft, The hydrogen liquids, *J. Phys.: Condens. Matter* **12**, A129 (2000).
- [38] Y. Katayama, T. Mizutani, W. Utsumi, O. Shimomura, M. Yamakata, and K.-i. Funakoshi, A first-order liquid–liquid phase transition in phosphorus, *Nature (London)* **403**, 170 (2000).
- [39] G. Monaco, S. Falconi, W. A. Crichton, and M. Mezouar, Nature of the First-Order Phase Transition in Fluid Phosphorus at High Temperature and Pressure, *Phys. Rev. Lett.* **90**, 255701 (2003).
- [40] S. Ohnishi, A theory of the pressure-induced high-spin-low-spin transition of transition-metal oxides, *Phys. Earth Planet. Inter.* **17**, 130 (1978).

- [41] S. Ohnishi and S. Sugano, Strain interaction effects on the high-spin-low-spin transition of transition-metal compounds, *J. Phys. C* **14**, 39 (1981).
- [42] T. Kambara, Theory of high-spin low-spin transitions in transition metal compounds induced by cooperative molecular distortions and lattice strains, *J. Chem. Phys.* **74**, 4557 (1981).
- [43] M. Ross and F. Rogers, Polymerization, shock cooling, and the high-pressure phase diagram of nitrogen, *Phys. Rev. B* **74**, 024103 (2006).
- [44] F. A. Gorelli, S. De Panfilis, T. Bryk, L. Ulivi, G. Garbarino, P. Parisiades, and M. Santoro, Simple-to-complex transformation in liquid rubidium, *J. Phys. Chem. Lett.* **9**, 2909 (2018).
- [45] H. Ogura, H. Matsuda, T. Ogawa, N. Ogita, and A. Ueda, Computer simulation for the melting curve maximum phenomenon: Two-species soft-core model, *Prog. Theor. Phys.* **58**, 419 (1977).
- [46] D. A. Young and B. J. Alder, Melting-Curve Extrema from a Repulsive “Step” Potential, *Phys. Rev. Lett.* **38**, 1213 (1977).
- [47] G. Jackson, W. G. Chapman, and K. E. Gubbins, Phase equilibria of associating fluids, *Mol. Phys.* **65**, 1 (1988).
- [48] P. Hopkins, A. J. Archer, and R. Evans, Pair-correlation functions and phase separation in a two-component point Yukawa fluid, *J. Chem. Phys.* **124**, 054503 (2006).
- [49] E. Rapoport, Melting-curve maxima at high pressure. II. Liquid cesium. resistivity, Hall effect, and composition of molten tellurium, *J. Chem. Phys.* **48**, 1433 (1968).
- [50] E. Gregoryanz, O. Degtyareva, M. Somayazulu, R. J. Hemley, and H.-k. Mao, Melting of Dense Sodium, *Phys. Rev. Lett.* **94**, 185502 (2005).
- [51] V. V. Kechin, Melting curve equations at high pressure, *Phys. Rev. B* **65**, 052102 (2001).
- [52] G. D. Mukherjee and R. Boehler, High-Pressure Melting Curve of Nitrogen and the Liquid-Liquid Phase Transition, *Phys. Rev. Lett.* **99**, 225701 (2007).
- [53] A. Cadien, Q. Y. Hu, Y. Meng, Y. Q. Cheng, M. W. Chen, J. F. Shu, H. K. Mao, and H. W. Sheng, First-Order Liquid-Liquid Phase Transition in Cerium, *Phys. Rev. Lett.* **110**, 125503 (2013).
- [54] E. Rapoport, Model for melting-curve maxima at high pressure, *J. Chem. Phys.* **46**, 2891 (1967).
- [55] M. Dijkstra and D. Frenkel, Evidence for Entropy-Driven Demixing in Hard-Core Fluids, *Phys. Rev. Lett.* **72**, 298 (1994).
- [56] G. Makov and E. Yahel, Liquid-liquid phase transformations and the shape of the melting curve, *J. Chem. Phys.* **134**, 204507 (2011).
- [57] Y. Shor, E. Yahel, and G. Makov, Short range order in anomalous liquid metals, *J. Non-Cryst. Solids* **358**, 2687 (2012).
- [58] J. L. Dye, Electrides: Ionic salts with electrons as the anions, *Science* **247**, 663 (1990).
- [59] P. K. Ahluwalia, S. J. Clark, and G. J. Ackland, Structural phase transitions in calcium: A first principle calculation, in *Solid State Physics: Proceedings of the DAE Solid State Physics Symposium*, Vol. 41 (Universities Press, Hyderabad, 1998), p. 147.
- [60] C. J. Pickard and R. J. Needs, Dense Low-Coordination Phases of Lithium, *Phys. Rev. Lett.* **102**, 146401 (2009).
- [61] J.-Y. Raty, E. Schwegler, and S. A. Bonev, Electronic and structural transitions in dense liquid sodium, *Nature (London)* **449**, 448 (2007).
- [62] B. Rousseau, Y. Xie, Y. Ma, and A. Bergara, Exotic high pressure behavior of light alkali metals, lithium and sodium, *Eur. Phys. J. B* **81**, 1 (2011).
- [63] Y. Li, Y. Wang, C. J. Pickard, R. J. Needs, Y. Wang, and Y. Ma, Metallic Icosahedron Phase of Sodium at Terapascal Pressures, *Phys. Rev. Lett.* **114**, 125501 (2015).
- [64] M.-s. Miao and R. Hoffmann, High-pressure electrides: The chemical nature of interstitial quasiatoms, *J. Am. Chem. Soc.* **137**, 3631 (2015).
- [65] Z. Yu, H. Y. Geng, Y. Sun, and Y. Chen, Optical properties of dense lithium in electride phases by first-principles calculations, *Sci. Rep.* **8**, 3868 (2018).
- [66] S. F. Elatresh, Z. Zhou, N. W. Ashcroft, S. A. Bonev, J. Feng, and R. Hoffmann, High-pressure lithium as an elemental topological semimetal, *Phys. Rev. Mater.* **3**, 044203 (2019).
- [67] R. Paul, S. X. Hu, V. V. Karasiev, S. A. Bonev, and D. N. Polsin, Thermal effects on the electronic properties of sodium electride under high pressures, *Phys. Rev. B* **102**, 094103 (2020).
- [68] S. Ayrihac, V. Naden-Robinson, F. Decremps, M. Gauthier, D. Antonangeli, S. Scandolo, and M. Morand, High-pressure transformations in liquid rubidium, *Phys. Rev. Mater.* **4**, 113611 (2020).
- [69] W. L. Bragg and E. J. Williams, The effect of thermal agitation on atomic arrangement in alloys, *Proc. R. Soc. London Ser. A* **145**, 699 (1934).
- [70] T. Tsuchiya, R. M. Wentzcovitch, C. R. S. da Silva, and S. de Gironcoli, Spin Transition in Magnesiowüstite in Earth’s Lower Mantle, *Phys. Rev. Lett.* **96**, 198501 (2006).
- [71] M. L. Marcondes, F. Zheng, and R. M. Wentzcovitch, Phonon dispersion throughout the iron spin crossover in ferropiclasite, *Phys. Rev. B* **102**, 104112 (2020).
- [72] T. Tsuchiya, R. M. Wentzcovitch, C. R. Da Silva, S. De Gironcoli, and J. Tsuchiya, Pressure induced high spin to low spin transition in magnesiowüstite, *Phys. Status Solidi (b)* **243**, 2111 (2006).
- [73] J.-F. Lin, V. V. Struzhkin, S. D. Jacobsen, M. Y. Hu, P. Chow, J. Kung, H. Liu, H.-k. Mao, and R. J. Hemley, Spin transition of iron in magnesiowüstite in the earth’s lower mantle, *Nature (London)* **436**, 377 (2005).
- [74] C. McCammon, I. Kantor, O. Narygina, J. Rouquette, U. Ponkratz, I. Sergueev, M. Mezouar, V. Prakapenka, and L. Dubrovinsky, Stable intermediate-spin ferrous iron in lower-mantle perovskite, *Nat. Geosci.* **1**, 684 (2008).
- [75] Y. Sun, M. Cococcioni, and R. M. Wentzcovitch, LDA+ $U_{sc}$  calculations of phase relations in FeO, *Phys. Rev. Mater.* **4**, 063605 (2020).
- [76] R. Wentzcovitch, J. Justo, Z. Wu, C. R. da SILVA, D. Yuen, and D. Kohlstedt, Anomalous compressibility of ferropiclasite throughout the iron spin cross-over, *Proc. Natl. Acad. Sci.* **106**, 8447 (2009).
- [77] M. Dijkstra, D. Frenkel, and J.-P. Hansen, Phase separation in binary hard-core mixtures, *J. Chem. Phys.* **101**, 3179 (1994).
- [78] M. Dijkstra, R. van Roij, and R. Evans, Phase Behavior and Structure of Binary Hard-Sphere Mixtures, *Phys. Rev. Lett.* **81**, 2268 (1998).
- [79] V. Holten and M. Anisimov, Entropy-driven liquid–liquid separation in supercooled water, *Sci. Rep.* **2**, 713 (2012).
- [80] L. F. Lundegaard, M. Marqués, G. Stinton, G. J. Ackland, R. J. Nelmes, and M. I. McMahon, Observation of the

- oP8* crystal structure in potassium at high pressure, *Phys. Rev. B* **80**, 020101(R) (2009).
- [81] L. F. Lundegaard, G. W. Stinton, M. Zelazny, C. L. Guillaume, J. E. Proctor, I. Loa, E. Gregoryanz, R. J. Nelmes, and M. I. McMahon, Observation of a reentrant phase transition in incommensurate potassium, *Phys. Rev. B* **88**, 054106 (2013).
- [82] S. Falconi and G. J. Ackland, *Ab initio* simulations in liquid caesium at high pressure and temperature, *Phys. Rev. B* **73**, 184204 (2006).
- [83] H. Li, H. Ding, Y. Tian, Y. L. Sun, and M. Li, Regularities of liquid potassium at different temperatures, *AIP Adv.* **9**, 075018 (2019).
- [84] G. J. Ackland, M. Dunuwille, M. Martinez-Canales, I. Loa, R. Zhang, S. Sinogeikin, W. Cai, and S. Deemyad, Quantum and isotope effects in lithium metal, *Science* **356**, 1254 (2017).
- [85] T. Matsuoka and K. Shimizu, Direct observation of a pressure-induced metal-to-semiconductor transition in lithium, *Nature (London)* **458**, 186 (2009).
- [86] M. Hanfland, K. Syassen, N. E. Christensen, and D. L. Novikov, New high-pressure phases of lithium., *Nature (London)* **408**, 174 (2000).
- [87] C. Ji, B. Li, W. Liu, J. S. Smith, A. Majumdar, W. Luo, R. Ahuja, J. Shu, J. Wang, S. Sinogeikin *et al.*, Ultrahigh-pressure isostructural electronic transitions in hydrogen, *Nature (London)* **573**, 558 (2019).
- [88] G. J. Ackland and J. S. Loveday, Structures of solid hydrogen at 300 K, *Phys. Rev. B* **101**, 094104 (2020).
- [89] H. Schmider and A. Becke, Chemical content of the kinetic energy density, *J. Mol. Struct (THEOCHEM)* **527**, 51 (2000).
- [90] S. J. Clark, M. D. Segall, C. J. Pickard, P. J. Hasnip, M. I. J. Probert, K. Refson, and M. C. Payne, First principles methods using CASTEP, *Z. Kristall.* **220**, 567 (2005).